The generation of crystal-poor rhyolites in the upper crust

Eva Hartung, Luca Caricchi

Department of Earth Sciences, University of Geneva, Rue des Maraîchers 13, 1205 Geneva, Switzerland

Corresponding authors:

Eva Hartung email: eva.hartung@unige.ch

Keywords: rhyolite-MELTS, silicic volcanism, water content, melt extraction, hindered settling, Takidani pluton

ABSTRACT

The extraction of felsic melts, from crystallizing crustal magma reservoirs, is essential for the chemical evolution of the crust and is a phenomenon preceding some of the largest eruptions on Earth. The physical properties of residual melt and magma and the time at which the conditions remain appropriate for melt extraction are the most important factors controlling the efficiency of melt extraction and the distribution of melt in magma reservoirs. We use rhyolite-MELTS simulations to evaluate the physical evolution of crystallizing granodioritic (or dacitic) hydrous magma (i.e. ≥1 wt.% H_2O) at 200 MPa. These results allow us to estimate extraction velocities of residual melt and to identify the optimal conditions at which melt segregation occurs. We additionally estimate the time that magma reservoirs of different thicknesses spend within the window that is best suited for magma extraction. Hydrous magmas that attain water saturation after 40 wt.% crystallization (rheological locking point) are best suited for melt extraction. In

fact, once water-saturation is achieved, the rate of release of latent heat of crystallization increases while the viscosity of the residual liquid and crystal-liquid density contrast remain favorable for melt segregation. We test our findings on the Takidani pluton (Japan) because it shows clear evidences of residual melt segregation from crystallizing magma, and was associated with caldera-forming eruptions. In agreement with geochemistry, the calculations show that most of the melt-rich body at the top of the pluton was formed once the pluton crystallized to 40-50 wt.% and water-saturation was achieved. Estimates of the duration of cooling in this system suggest that residual melt properties were appropriate to allow the formation of a single melt-rich lens at the top of the reservoir. Our results can be generalized to upper crustal magma reservoirs and suggest that sufficiently large upper crustal reservoirs containing granodioritic (i.e. dacitic) magma with more than 3 wt.% H_2O can produce large melt-rich caps at the top of partially crystallized magma within relatively short timescales. In H_2O-poorer magmas the time available for melt extraction is not sufficient for complete extraction of the residual melt, which, therefore, accumulates in isolated pockets. The tendency of water-poorer magmas to form melt-rich lenses within partially crystallized magma may decrease our capacity of detecting eruptible magma using geophysical methods in volcanic systems such as Yellowstone.

1. Introduction

1.1. Crystal-liquid separation in the upper crust

Segregation of interstitial melt from a rheologically-locked partially-crystallized magma has been proposed by various authors as a potential mechanism for the generation of shallow and voluminous reservoirs of crystal-poor and eruptible rhyolite (Bachmann and Bergantz, 2004; Dufek and Bachmann, 2010; Hildreth, 2004, 1981; Hildreth and Wilson, 2007; Marsh, 1981).

Thermo-mechanical simulations suggest that the efficiency of melt extraction for common hydrous silicic magma compositions is highest at crystal contents between 50% and 70% (Dufek and Bachmann, 2010). These studies also emphasize that the probability for interstitial melt extraction is not only controlled by the physical properties of residual melt and magma, but by the time spent by magma at conditions best suited for melt extraction (Dufek and Bachmann, 2010; Huber et al., 2009). This, in turn, is function of the topology of the phase diagram, specifically of the rate of latent heat release during progressive cooling, and evolution of the physical properties of the residual melt of magma with increasing crystallinity (Caricchi and Blundy, 2015; Huber et al., 2009; Lee et al., 2015; Melekhova et al., 2013). The results of these studies permit to draw some general conclusions about extraction of residual melt in felsic systems: i) Independently of the process leading to the extraction of residual melt in crystallizing felsic magmas, the separation between residual melt and crystals occurs when magma is rheologically locked (i.e. crystal fraction >0.4; Dufek and Bachmann, 2010; Huber et al., 2010; Marsh, 1981; Pistone et al., 2015); ii) The velocity of residual melt extraction is directly proportional to the ratio between the density difference of crystals and residual melt and the viscosity of the residual melt (Bachmann and Bergantz, 2004; Dufek and Bachmann, 2010) ; iii) The longer magma spends at conditions suitable for residual melt extraction, the larger is the amount of residual melt extracted (Dufek and Bachmann, 2010; Huber et al., 2009).

Evidences for large-scale segregation of rhyolitic melts is commonly retrieved from volcanic sequences (Bachmann and Bergantz, 2004; Deering et al., 2011; Hildreth and Wilson, 2007), however, such testimony is scarce or obscure in the intrusive record (Coleman et al., 2004; Gelman et al., 2014; Vigneresse, 2014). The Takidani pluton is texturally zoned, with a gradual transition (over about 50 m) from equigranular to porphyritic texture (Fig. 1). The whole

rock chemistry of the equigranular (GDT) and the porphyritic portions (pGT) of the intrusion, suggest that pGT was extracted from GDT once the residual melt fraction dropped to 40-50 wt.% (Figs. 1, 2a; Hartung et al., 2017). These findings are confirmed by trace element analyses carried out on plagioclase (Fig. 2b). Additionally, the composition, mineral chemistry and age, of the Takidani pluton and volcanic products distributed across Japan are similar, which supports the hypothesis that the Takidani pluton fed volcanic activity (Kataoka et al., 2001; Kimura and Nagahashi, 2007). This makes the Takidani pluton an excellent candidate to investigate the formation of shallow rhyolitic reservoirs and the build-up to large caldera-forming eruptions. In this study, we calculate the variation of the physical properties of magma and residual melt for granodioritic (i.e. dacitic) magmas that are comparable to those of the Takidani pluton, for a range of initial water contents (H_2O_i) between 1 and 6 wt.%. We aim 1) to constrain the effect of H_2O_i content on the efficiency of melt extraction, 2) to identify the conditions that led to the extraction of residual melt from the Takidani pluton, and 3) to define the impact of H_2O_i content on the architecture of upper crustal magma reservoirs.

2. Material and methods

2.1. Rhyolite-MELTS

Existing experimental data do not cover the entire range of temperature and water content required to trace the evolution of residual melt during cooling and crystallization of magma in the upper crust (Costa et al., 2004; Holtz et al., 2005; Scaillet and Evans, 1999). Thus, we use rhyolite-MELTS (Gualda et al., 2012) to calculate the chemical and physical evolution of residual melt of granodioritic magma from liquidus to solidus temperature and over the entire range of initial water content between 1 and 6 wt.%. Because granodiorites represent about 95

93 wt.% of the upper crust (Rudnick and Gao, 2003) and because the main portion of the Takidani
94 pluton is granodioritic with a composition similar to the starting material of Costa et al. (2004;
95 Hartung et al., 2017), we use this composition for the rhyolite-MELTS calculations. This
96 composition also allows us to test the performance of rhyolite-MELTS, especially in reproducing
97 the residual melt compositions produced experimentally by Costa et al. (2004).
98 In our rhyolite-MELTS simulations we force crystallization by removing an equal
99 amount of heat from the system (i.e. 1 J/g) at each step (*n*) starting from the liquidus temperature
100 down to a temperature (*T*) of about 740°C, which corresponds to a residual melt fraction of about
101 0.1. With this approach, we assume that a fix rate of heat is being released from the magma (i.e.
102 constant heat loss). Thus, the number of modeling steps within a given temperature interval
103 becomes proportional to the time spent by the magma within that interval of temperature. This is
104 important to be able to quantify the total time that magma spends within the temperature and
105 crystallinity range at which residual melt extraction occurs (Dufek and Bachmann, 2010).
106 For all calculations, the confining pressure was fixed at 200 MPa, which are the
107 conditions applied in the Costa et al. (2004) experiments and are close to the inferred
108 emplacement depth for the Takidani pluton (Hartung et al., 2017). The oxygen fugacity was
109 initially fixed to the nickel-nickel oxide buffer (NNO) to calculate the liquidus temperature (for
110 different H_2O_i), but remained unconstrained during progressive heat extraction. Although
111 rhyolite-MELTS does not capture all subtleties of the phase equilibria for hydrous magmas (i.e.
112 amphibole and biotite crystallization), the residual melt composition varies as function of
113 temperature and water content following the experimental residual liquids of the experiments of
114 Costa et al. (2004; Fig.3).
115

2.2. *The Takidani pluton: evidences of melt segregation and eruption*

In the following we provide a summary of the main results of a geochemical study previously performed on the Takidani pluton (Hartung et al., 2017). The Takidani pluton is a well exposed and extremely young pluton (1.63 Ma, Ito et al., 2017), located in the Central Japan Alps and it is thought to present the source of voluminous dacitic and rhyolitic eruptions at the Plio-Pleistocene boundary (Kimura and Nagahashi, 2007). The pluton is vertically exposed over 1800 m (Fig. 1; Harayama et al., 2003) from a tectonic contact at the base to a magmatic roof contact with older volcanic lithology (i.e. Hotaka Andesite, Harayama, 1994). Textural, chemical and isotopic evidence of large-scale melt segregation is observed in the upper part of the pluton (Figs. 1,2; Hartung et al., 2017). The rock textures of the Takidani pluton change from holocrystalline to progressively more porphyritic appearance from the base and center to the roof of the intrusion. Major and trace element whole rock analysis and data obtained through quantitative evaluation of minerals by QEMSCAN and electron microprobe analyses (EMPA) are used to determine the area percent and chemical composition of the matrix components (equivalent to residual melt composition) throughout the upper section of the Takidani pluton (Fig. 1). This data shows a progressive increase in the residual melt components defined by quartz (Qtz), alkali feldspar (Kspar) and albite-rich plagioclase (Plg<An30) from the equigranular granodiorite (GDT) to the porphyritic granite (pGT; Fig. 1). However, the relative fraction of quartz (Qtz), albite (Ab), and orthoclase (Or) and therefore the melt compositions remains constant across the textural and chemical transition and suggest that the residual melt had a chemical composition equivalent to the granitic minimum at approximately 200 MPa (Johannes and Holtz, 1996).

Hartung et al. (2017) show that magmatic differentiation in the Takidani pluton is dominated by crystal fractionation with minor assimilation of older partially molten granite (Fig. 2a). Concentrations of Rb in plagioclase increases from core to rim and can be modeled with the crystallization of magma to more than 50 wt.% (Fig. 2b). All plagioclases are characterized by a common rim, which formed when the magma crystal fraction reached 40-50 wt.%. The ubiquitous presence of such plagioclase rims indicates that the magma reached its rheological locking point at this crystallinity (Fig. 2b). Additionally, petrographic observations suggest that plagioclase started crystallizing at temperatures of about 900-850°C and before amphibole reached its liquidus temperature (~850°C). The distribution of temperature estimates in amphibole and comparison to phase equilibria experiments from Costa et al. (2004) highlight that amphibole dominantly grew under low temperature conditions (<800°C, Hartung et al., 2017) and crystallinities of >40 wt.%, which again corresponds to the rheological locking of crystal mushes (Caricchi et al., 2007; Pistone et al., 2013). The late appearance of amphibole thus not only indicates emplacement and crystallization at pressure of about 200 MPa, but that the initial water content of the granodioritic magma was between 3 and 4 wt.% and that the extraction of residual melt from the crystallizing magma occurred under water saturated conditions (Costa et al., 2004; Hartung et al., 2017). These evidences show that the pGT unit represents a lens of residual melt extracted from the underlying GDT granodiorite.

3. Results

3.1. Thermal, chemical and physical evolution of dacitic magma

Water has an important effect on phase equilibria as it depresses liquidus temperatures and modifies the relationships between crystallinity, physical properties of magmas and temperature

(e.g. viscosity and density of the residual melt ; Caricchi et al., 2007; Giordano et al., 2008; Lange, 1994; Melekhova et al., 2013; Whitney, 1988). The extraction of heat from a magma reservoir forces its crystallization and causes silica and water enrichment in the residual melt (Fig. 4). Once the residual melt becomes water saturated, H_2O_i-undersaturated magmas join the *T*-crystallinity trajectory of H_2O_i-saturated magma (Fig. 4). At 200 MPa the liquidus temperature of granodioritic (or dacitic) magma with an initial water content of 1 wt.% lies at 1080°C (rhyolite-MELTS), while the liquidus temperature of water saturated (about 6 wt% H_2O; Ghiorso and Gualda, 2015) dacitic magma is 110°C lower (Fig. 5a). Such difference in liquidus temperature implies that relatively drier magmas have a higher initial heat content with respect to water-bearing magmas, thus, leading to longer cooling periods. Moreover, the initial water content affects the relationship between temperature and crystallinity of magma (Fig. 5a; Whitney, 1988). The rate of crystallization is non-linear for hydrous magmas. Thus, the rate of latent heat release is not constant and in a system in which heat is extracted at approximately constant rate, magma spends the largest amount of time at temperatures where the rate crystallization (i.e. rate of latent heat release) is highest (Caricchi and Blundy, 2015; Marsh, 1981). Water also affects the evolution of density contrast between crystals and residual melt and the viscosity of the residual melt within the rheologically locked region, which, in turn, modulates the velocity of residual melt extraction (Figs. 5b, c; Bachman and Bergantz, 2004). Regardless of the initial water content of the magma, residual melt viscosity increases down to melt fractions of 0.5-0.4 because of decreasing temperature and increasing silica content. At lower melt fractions (<0.4) and once volatile saturation is achieved, the viscosity of the residual melt remains unchanged independent of the initial water content (Fig. 5b). Relatively dry melts ($H_2O_i \leq 2$ wt.%) reach a maximum in viscosity before joining the viscosity-temperature path at

low melt fractions (Fig. 5b). The contrast in density between the solid phase and residual melt spans a wide range of values near liquidus conditions (for different H_2O_i) but becomes less dependent on H_2O_i for melt fractions <0.6 (Fig. 5c). The ratio of the difference in density between crystals and residual melt and the viscosity of the residual melt, which is directly related to the velocity of melt extraction (Bachman and Bergantz, 2004), generally increases with water content (Figs. 5b, c).

Based on the above and when considering only the physical properties of the residual melt, the extraction velocity of residual melt is the fastest for H_2O_i-saturated magmas. However, the total time spent by magma at melt fractions <0.6 (i.e. rheologically locked conditions) is inversely proportional to the initial water content of magma (Fig. 5d). To assess the relative importance of the initial water content on the physical properties of magma and the timescales available for melt segregation to occur, we calculate the velocity of melt extraction by hindered settling for granodioritic-dacitic magma throughout the rheologically locked portion of the magmatic cooling history (melt fraction<0.6). As the velocity of residual melt extraction depends importantly on the process and the physical properties of crystals and residual melt (Bachmann and Bergantz, 2004), the timescales and velocity of melt extraction provided here should be considered as first order estimate. We further notice that the process of residual melt extraction in this formulation is simplified but we are interested in the comparison between the efficiency of residual melt for magmas with different initial water contents. Compaction or gas-filter pressing are viable mechanisms but an accurate analysis of the mechanisms responsible for the extraction of residual melt is beyond the scope of this contribution.

3.2. Timescales of melt segregation

We use the physical properties obtained from rhyolite-MELTS simulations to calculate hindered settling velocities (U_{hs}) for crystallizing magma reservoirs (i.e. Takidani pluton) following the equation provided by Bachmann and Bergantz (2004):

$$U_{hs} = \frac{2r^2 g \Delta\rho}{9\mu} \frac{(1-c)^2}{(1+c^{1/3})^{[5c/3(1-c)]}} \quad (1)$$

Where r is the crystal radius, g is gravitational acceleration (9.81 ms^{-1}), $\Delta\rho$ is the density difference between crystal and melt, μ is the viscosity of the melt and c is the crystal fraction. Crystal fraction and size control porosity and permeability of silicic mushes (McKenzie, 1984), and can affect melt extraction velocity by several orders of magnitude (Bachmann and Bergantz, 2004). To compare the velocities obtained for magmas with different H_2O_i, we always consider a crystal radius of 3 mm, which is appropriate for the Takidani pluton (Fig. 1; Hartung et al., 2017). Settling velocities vary between 3.0 and 0.02 m/yr for melt fractions decreasing from 0.6 to 0.2 (Fig. 6). Segregation velocities for $H_2O_i \geq 3$ wt.%, i.e. within the rheologically locked interval remain essentially the same because the residual melt at these crystallinities is water saturated (Fig. 6). Magmas with $H_2O_i < 3$ wt.%, however, become water saturated at lower temperature and at higher crystallinities resulting in much slower settling velocities mainly because of their higher viscosity. Based on these calculations, the residual melt separates more efficiently from highly crystallized dacitic magmas if the initial water concentration is equal or greater than 3 wt.%. It is important to stress that these conclusions are valid for a confining pressure of 200 MPa. Water solubility in magma increases with pressure, thus, at higher pressure the threshold of H_2O_i at which the increase of segregation efficiency occurs is higher.

229 The relative amount of melt that can be extracted depends on the time period that magma
230 spends within the rheologically locked temperature interval, which, in turn, is function of magma
231 temperature and the crystallization rate (i.e. rate of release of latent heat of crystallization) within
232 the rheologically locked interval. For $H_2O_i \leq 3$ wt.% the average magma temperature within the
233 rheologically locked interval increases (Fig. 5a). When H_2O_i-undersaturated magmas reach
234 volatile saturation, the rate of crystallization sharply increases resulting in an increase of the rate
235 of release of latent heat of crystallization (Fig. 5a; Marsh, 1981, Caricchi and Blundy, 2015b).
236 Magmas that formed the Takidani pluton were initially H_2O-undersaturated with water contents
237 of about 3 to 4 wt.% (Hartung et al., 2017; Costa et al., 2004). The residual melt would have
238 reached volatile saturation at melt fractions of about 0.70 to 0.55 and temperatures around 820°C
239 to 780°C (Fig. 5a,b), at which point an increase of crystallization rate, enhanced release of latent
240 heat of crystallization, and decreased magma cooling rates are expected. This is confirmed by
241 amphibole thermometry, as the largest number of amphiboles measured in the granodiorite
242 portion of the Takidani intrusion suggest prolonged residence within a relatively narrow
243 temperature interval below 800°C (Hartung et al., 2017).
244 Our rhyolite-MELTS calculations and experimental phase relationships (Costa et al.,
245 2004) indicate that the Takidani pluton initially contained about 3 to 4 wt.% H_2O and spent a
246 relatively large fraction of its cooling timescale at melt fractions <0.65 (Fig. 5d). The interplay
247 between the viscosity of the residual melt, the density contrast between residual melt and
248 crystals, and the time spent within the rheologically locked crystallinity interval, favored the
249 extraction of residual melt from the Takidani pluton (Fig. 5).
250 In the following we investigate how the initial amount of water dissolved in magma can
251 affect the architecture of partially crystallized dacitic reservoirs. More specifically we calculate

252 the potential for the formation of melt-rich rhyolitic lenses within partially crystallized magma,
253 or caps at the roof of magma reservoirs (Bachmann and Bergantz, 2004; Wotzlaw et al., 2014).
254
255 4. Discussion
256 4.1. *Application to the Takidani pluton*
257 We estimate the time required for magma to cool to a crystal fraction of 0.1 by 1) considering the
258 total enthalpy content (from rhyolite-MELTS) of a magmatic reservoir constituted of fully
259 molten granodioritic magma and 2) removing heat by applying a constant heat loss per surface
260 area. For a fixed volume, reservoirs with high aspect ratios (i.e. diameter to thickness ratio) have
261 larger surface area and, thus, cool faster. The time available for melt migration is equal to the
262 time the magma spends within the rheologically locked temperature range. The distance travel by
263 the melt is the cumulative sum of the hindered settling velocity calculated for each temperature
264 range, multiplied by the time the magma spends within each temperature range.
265 For the Takidani Pluton, we consider a cylindrical shape and a volume of 80 km^3 with a
266 radius of 6.5 km (i.e. 13 km length; Harayama, 1992) and mush thickness of 0.6 km (i.e. GDT
267 and pGT units, Hartung et al. 2017). These are the dimensions of the exposed portion of the
268 pluton and are therefore minimum reservoir volume estimates. The observed column of extracted
269 melt (h) corresponds to the pGT unit in the upper part of the pluton (270 m; Fig. 1, Hartung et al.
270 2017). The total amount of enthalpy available for the Takidani reservoir for a dacitic
271 composition, a fixed bulk density of 2500 kg/m^3 and initial water content of 3 and 4 wt.% is 3.1
272 and 2.8 x 10^{19} J, respectively. To estimate the cooling timescale from the liquidus to a
273 temperature corresponding to a melt fraction of 0.1, we use a constant heat loss of 2 $J/s/m^2$,
274 which is comparable to average heat flow measurements at Yellowstone Caldera (DeNosaquo et

al., 2009). Cooling from liquidus to a melt fraction of 0.1 for such reservoir geometry, would have been completed in 1500-1700 years for magmas with initial water contents of 4 to 3 wt.%, respectively. We normalize these cooling timescales to the number of simulation steps from rhyolite-MELTS to calculate the time magma spent within each simulation step. By multiplying the time within each step by the corresponding hindered settling velocity for the corresponding temperature (Fig. 6), we calculate the distance travel by the melt while the magma was in a rheologically locked state (i.e. 0.6-0.2 melt fraction). Rhyolite-MELTS simulations in combination with our estimates of cooling timescales show that the segregation of the 270 m pGT unit occurred over 220 -160 years. Such timescales indicate that the extraction of residual melt is a relatively fast process that currently cannot be resolved with geochronology (e.g. Wotzlaw et al., 2014). Velocities of melt extraction about one order of magnitude slower (see compaction velocities with respect to hindered settling in Bachmann and Bergantz, 2004) would not lead to the formation of a melt-rich cap in the Takidani Pluton. Using the approach applied to the Takidani pluton, in the following we estimate the potential amount of residual melt extracted from magma reservoirs of different volumes containing dacitic magma with different initial H_2O content (1-6 wt.%).

4.2. The control of H_2O_i on the extraction of residual melt from crystallizing magmas

Geochemical and petrologic studies show that crystal poor rhyolites are sourced either from caps at the top of partially crystallized reservoirs (Bachmann and Bergantz, 2004; Hildreth and Wilson, 2007), or from the amalgamation of isolated melt pockets dispersed within a highly crystallized magma (Wotzlaw et al., 2014, Ellis et al., 2014). However, the processes responsible for the generation of reservoirs with such distinct architecture are not yet fully understood.

298 Considering the extraction of residual melt by any physical process, the final distribution of
299 crystal-poor melt will be determined by the total distance the melt can travel before the system
300 cools to its solidus temperature. Thermally, the maximum amount of crystal-poor melt that can
301 potentially be accumulated depends mainly on the mass of magma within a magmatic system
302 (i.e. heat content) and on its volume to surface ratio (rate of heat loss; Fig. 7). Our results show
303 that chemically, the initial amount of water dissolved in dacitic magmas affects both the total
304 amount of time magmas spend within the rheologically locked temperature interval and the
305 velocity of residual melt extraction from crystallizing magmas (Figs. 5d, 6, 7). To identify which
306 magma compositions are best suited for the formation of melt caps or lenses, we first calculate
307 the cooling timescale by considering a constant heat loss of 2 J/s/m^2 for dacitic magmas with
308 different H_2O_i for reservoirs of different volume and aspect ratio volumes (volume = 10^2-10^4 km^3
309 and thicknesses 1-5 km). We assume that a melt-rich cap forms at the top of the reservoir if
310 segregation velocities and time within the rheologically locked temperature window are
311 sufficiently high for the residual melt to reach the top of the reservoir before the magma reaches
312 a crystal fraction of 0.8. Hence, to extract fifty percent of residual melt, the calculated
313 segregation distance needs to be half of the thickness of the magma reservoir. If less melt is
314 extracted the residual melt needs to travel further. If velocities are lower or if reservoir aspect
315 ratios are low (i.e. horizontally extended reservoirs), the melt does not reach the roof of the
316 magma reservoir before cooling to 80 wt.% crystals. In this case we consider that isolated melt-
317 rich pockets form within a highly crystallized magma.

318 Our calculations show that the residual melt of magmas containing more that 3 wt.%
319 H_2O_i moves greater distances in shorter timescales (Fig. 7) and are very likely to form crystal
320 rich caps at or near the roof of the magma reservoir (Fig. 8). Magmas with less than 2 wt.% H_2O_i

are unlikely to form any melt-rich body independent of the size or thickness of the magma reservoir (Figs. 7,8). Although magmas with 1 wt.% H_2O_i spent half of their cooling time within the rheological locking temperature window, because of the high viscosity of the residual melt (i.e. low extraction velocity) they tend not to form caps or melt-rich lenses of crystal poor rhyolite. The boundaries between caps and lenses depend on the segregation velocity of the residual melt. Slower segregation of the residual melt, for instance through compaction or hindered settling in magma with smaller crystals (< 3mm radius; Bachmann and Bergantz, 2004), will decrease the probability of forming caps of crystal-poor rhyolitic melt and expand the field appropriate for the formation of isolated melt-rich lenses.

5. Conclusions

The Takidani magmatic reservoir formed, what appears to be, a cap of segregated residual melt near the roof of the magmatic reservoir (Hartung et al., 2017). With an estimated initial water content of 3-4 wt.% and a thickness of 0.6 km, segregation of the residual melt to form the 270m thick pGT unit would have occurred between 220 and 160 years. The fact, that the Takidani pluton shows evidence of large-scale melt segregation may be associated with its water undersaturation at time of emplacement, which prolonged the time spent within the rheologically locked temperature range (Fig. 5d).

H_2O_i appears to have a pronounced impact on the potential of formation of crystal-poor melt caps or separate melt pockets. Dacitic magma mushes with $H_2O_i \geq 3$ wt.% are most likely to form large melt caps at the roof of a magma reservoir, while magmas with $H_2O_i < 3$ wt.% tends to form separate melt pockets due to slower segregation velocities. Magmas with $H_2O_i << 2$ wt.% are unlikely to show any signs of segregation of rhyolitic melts (Fig. 7).

Our calculations support the hypothesis that the porphyritic unit observed at the roof of the Takidani Pluton presents a melt-rich cap. Considering a thicker or more volumetric magma reservoir would strengthen this conclusion (Fig. 8). Our simplified model only considers constant heat diffusion across a fixed magma surface, however, it captures the fundamental parameters controlling the architecture of upper crustal magma reservoirs. The initial magma water content has a significant control on the potential of magma reservoir to form melt-rich caps or isolated melt pockets dispersed in a highly-crystallized magma. Our calculations suggest that while water rich magmas have the highest potential to form melt-rich caps, water poorer magma, as those typical of the Snake River Plane (USA), should have a higher tendency to form dispersed melt-rich lenses within magma mushes. This is in agreement with geochemical data, suggesting that eruptions in the Snake River Plane are fed by multiple melt-rich lenses (Wotzlaw et al., 2014, Ellis et al., 2014) and suggests that detection of eruptible magmas using geophysical methods, may be more complicated in H_2O-poor systems.

6. Acknowledgements

This work was supported by the Swiss National Fund [SNSF grant 200021_150204].

7. References

Bachmann, O., Bergantz, G., 2004. On the Origin of Crystal-poor Rhyolites : Extracted from Batholithic Crystal Mushes. J. Petrol. 45, 1565–1582. doi:10.1093/petrology/egh019

Caricchi, L., Blundy, J., 2015. Experimental petrology of monotonous intermediate magmas. Geol. Soc. London, Spec. Publ. doi:10.1144/SP422.9

Caricchi, L., BURLINI, L., ULMER, P., GERYA, T., VASSALLI, M., PAPALE, P., 2007. Non-

Newtonian rheology of crystal-bearing magmas and implications for magma ascent dynamics. Earth Planet. Sci. Lett. 264, 402–419. doi:10.1016/j.epsl.2007.09.032

Coleman, D.S., Gray, W., Glazner, A.F., 2004. Rethinking the emplacement and evolution of zoned plutons: Geochronologic evidence for incremental assembly of the Tuolumne Intrusive Suite, California. Geology 32, 433–436. doi:10.1130/G20220.1

Costa, F., Scaillet, B., Pichavant, M., 2004. Petrological and Experimental Constraints on the Pre-eruption Conditions of Holocene Dacite from Volcan San Pedro (36°S, Chilean Andes) and the Importance of Sulphur in Silicic Subduction-related Magmas. J. Petrol. 45, 855–881. doi:10.1093/petrology/egg114

Deering, C.D., Cole, J.W., Vogel, T.A., 2011. Extraction of crystal-poor rhyolite from a hornblende-bearing intermediate mush: A case study of the caldera-forming Matahina eruption, Okataina volcanic complex. Contrib. to Mineral. Petrol. 161. doi:10.1007/s00410-010-0524-0

DeNosaquo, K.R., Smith, R.B., Lowry, A.R., 2009. Density and lithospheric strength models of the Yellowstone–Snake River Plain volcanic system from gravity and heat flow data. J. Volcanol. Geotherm. Res. 188, 108–127. doi:10.1016/J.JVOLGEORES.2009.08.006

Dufek, J., Bachmann, O., 2010. Quantum magmatism: Magmatic compositional gaps generated by melt-crystal dynamics. Geology 38, 687–690. doi:10.1130/G30831.1

Ellis, B.S., Bachmann, O., Wolff, J. a., 2014. Cumulate fragments in silicic ignimbrites: The case of the Snake River Plain. Geology 42, 431–434. doi:10.1130/G35399.1

Gelman, S.E., Deering, C.D., Bachmann, O., Huber, C., Gutiérrez, F.J., 2014. Identifying the crystal graveyards remaining after large silicic eruptions. Earth Planet. Sci. Lett. 403, 299–306. doi:10.1016/j.epsl.2014.07.005

Ghiorso, M.S., Gualda, G. a. R., 2015. An H2O–CO2 mixed fluid saturation model compatible with rhyolite-MELTS. Contrib. to Mineral. Petrol. 169, 53. doi:10.1007/s00410-015-1141-8

Giordano, D., Russell, J.K., Dingwell, D.B., 2008. Viscosity of magmatic liquids: A model. Earth Planet. Sci. Lett. 271, 123–134. doi:10.1016/j.epsl.2008.03.038

Gualda, G.A.R., Ghiorso, M.S., Lemons, R. V., Carley, T.L., 2012. Rhyolite-MELTS: a Modified Calibration of MELTS Optimized for Silica-rich, Fluid-bearing Magmatic Systems. J. Petrol. 53, 875–890. doi:10.1093/petrology/egr080

Harayama, S., 1994. Cooling History of the youngest exposed pluton in the World - The Plio-Pleistocene Takidani Granodiorite (Japan Alps, central Japan). Mem. Geol. Soc. Japan 43, 87–97.

Harayama, S., Wada, H., Yamaguchi, Y., 2003. Trip A1 Quaternary and Pliocene granites in the Northern Japan Alps. Hutt. Symp. V, F. Guideb.

Hartung, E., Caricchi, L., Floess, D., Wallis, S., Harayama, S., Kouzmanov, K., Chiaradia, M., 2017. Evidence for residual melt extraction in the Takidani Pluton, Central Japan. J. Petrol. 58, 763–788. doi:10.1093/petrology/egx033

Hildreth, W., 2004. Volcanological perspectives on Long Valley , Mammoth Mountain , and Mono Craters : several contiguous but discrete systems. J. Volcanol. Geotherm. Res. 136, 169–198. doi:10.1016/j.jvolgeores.2004.05.019

Hildreth, W., 1981. Gradients in silicic magma chambers: Implications for lithospheric magmatism. J. Geophys. Res. Solid Earth 86, 10153–10192. doi:10.1029/JB086iB11p10153

Hildreth, W., Wilson, C.J.N., 2007. Compositional Zoning of the Bishop Tuff. J. Petrol. 48, 951–999. doi:10.1093/petrology/egm007

Holtz, F., Sato, H., Lewis, J., Behrens, H., Nakada, S., 2005. Experimental petrology of the

1991-1995 Unzen dacite, Japan. Part I: Phase relations, phase composition and pre-eruptive conditions. J. Petrol. 46, 319–337. doi:10.1093/petrology/egh077

Huber, C., Bachmann, O., Dufek, J., 2010. The limitations of melting on the reactivation of silicic mushes. J. Volcanol. Geotherm. Res. 195, 97–105. doi:10.1016/j.jvolgeores.2010.06.006

Huber, C., Bachmann, O., Manga, M., 2009. Homogenization processes in silicic magma chambers by stirring and mushification (latent heat buffering). Earth Planet. Sci. Lett. 283, 38–47. doi:10.1016/j.epsl.2009.03.029

Ito, H., Spencer, C.J., Danišík, M., Hoiland, C.W., 2017. Magmatic tempo of Earth's youngest exposed plutons as revealed by detrital zircon U-Pb geochronology. Sci. Rep. 7, 12457. doi:10.1038/s41598-017-12790-w

Johannes, W., Holtz, F., 1996. Petrogenesis and Experimental Petrology of Granitic Rocks. Springer-Verlag, Berlin, Heidelberg, New York.

Kataoka, K., Nagahashi, Y., Yoshikawa, S., 2001. An extremely large magnitude eruption close to the Plio-Pleistocene boundary: reconstruction of eruptive style and history of the Ebisutoge-Fukuda tephra, central Japan. J. Volcanol. Geotherm. Res. 107, 47–69. doi:10.1016/S0377-0273(00)00300-0

Kimura, J.-I., Nagahashi, Y., 2007. Origin of a voluminous iron-enriched high-K rhyolite magma erupted in the North Japan Alps at 1.75 Ma: Evidence for upper crustal melting. J. Volcanol. Geotherm. Res. 167, 81–99. doi:10.1016/j.jvolgeores.2007.02.004

Lange, R.A., 1994. The Effects of H2O, CO2 and F on the Density and Viscosity of Silicate Melts. Rev. Mineral. Geochemistry 30, 331–370.

Lee, C.-T.A., Morton, D.M., Farner, M.J., Moitra, P., 2015. Field and model constraints on

436 silicic melt segregation by compaction/hindered settling: The role of water and its effect on
437 latent heat release. Am. Mineral. 100, 1762–1777.
438 Marsh, B.D., 1981. On the crystallinity, probability of occurrence, and rheology of lava and
439 magma. Contrib. to Mineral. Petrol. 78, 85–98. doi:10.1007/BF00371146
440 McKenzie, D., 1984. The Generation and Compaction of Partially Molten Rock. J. Petrol. 25,
441 713–765. doi:10.1093/petrology/25.3.713
442 Melekhova, E., Annen, C., Blundy, J., 2013. Compositional gaps in igneous rock suites
443 controlled by magma system heat and water content. Nat. Geosci. 6, 385–390.
444 doi:10.1038/ngeo1781
445 Pistone, M., Arzilli, F., Dobson, K.J., Cordonnier, B., Reusser, E., Ulmer, P., Marone, F.,
446 Whittington, A.G., Mancini, L., Fife, J.L., Blundy, J.D., 2015. Gas-driven filter pressing in
447 magmas: Insights into in-situ melt segregation from crystal mushes. Geology 43, G36766.1.
448 doi:10.1130/G36766.1
449 Pistone, M., Caricchi, L., Ulmer, P., Reusser, E., Ardia, P., 2013. Rheology of volatile-bearing
450 crystal mushes: Mobilization vs. viscous death. Chem. Geol. 345, 16–39.
451 doi:10.1016/j.chemgeo.2013.02.007
452 Rudnick, R.L., Gao, S., 2003. Composition of the Continental Crust, in: Treatise on
453 Geochemistry. Elsevier, pp. 1–64. doi:10.1016/B0-08-043751-6/03016-4
454 Scaillet, B., Evans, B.W., 1999. The 15 June 1991 Eruption of Mount Pinatubo . I . Phase
455 Equilibria and Pre-eruption P–T–fO2–fH2O Conditions of the Dacite Magma. J. Petrol. 40,
456 381–411.
457 Vigneresse, J.-L., 2014. Textures and melt-crystal-gas interactions in granites. Geosci. Front.
458 doi:10.1016/j.gsf.2014.12.004

Whitney, J.A., 1988. The origin of granite: The role and source of water in the evolution of granitic magmas. Geol. Soc. Am. Bull. 100, 1886–1897.

Wotzlaw, J., Bindeman, I.N., Watts, K.E., Schmitt, A.K., Caricchi, L., Schaltegger, U., 2014. Linking rapid magma reservoir assembly and eruption trigger mechanisms at evolved Yellowstone-type supervolcanoes. Geology 42, 807–810. doi:10.1130/G35979.1

FIGURE CAPTIONS

Figure 1:

Evidence of melt segregation in the upper section of the Takidani Pluton. Variations of Rb/Sr whole-rock content from GDT to pGT and QEMSCAN images with interstitial quartz (pink), orthoclase (green) and plagioclase with anorthite content <30wt.% (red). All other abundant mineral phases (including plagioclase phenocrysts) are represented in different shades of grey. Interstitial quartz, alkali feldspar and plagioclase (An<30) are considered to represent the residual melt of the magma, which gradually increases from the equigranular GDT unit towards the porphyritic pGT unit. The values below the bars show the content of quartz, orthoclase and albite, normalized to a fraction of 1. These values remain relative constant and suggest that the residual melt composition was buffered at the granitic minimum (Johannes and Holtz, 1996).

Figure 2:

Crystal fractionation trends from whole-rock and mineral analyses; (a) Assimilation and fractional crystallization (AFC) models (Hartung et al., 2017) performed on whole rock analyses show that compositional diversity is dominantly produced by crystal fractionation. The grey dashed lines and numbers on the side show the amount of melt (i.e. 60 wt.%) and assimilation (i.e. 3.2 wt.%). (b) Concentrations of Rb in plagioclase phenocrysts increase from 0.54 to 1.31 ppm from core to rim, respectively, and point towards a progressive enrichment of the incompatible element Rb in the melt phase through crystal fractionation. The grey dashed lines and number below indicate the amount of melt fraction.

Figure 3:

Comparison between rhyolite-MELTS simulations (lines) and the matrix glass compositions (circles) measured between 950°C and 800°C by Costa et al. (2004). The color contouring indicates the initial water content of the starting material (Costa et al. 2004). Rhyolite-MELTS and experiments are in broad agreement and show the effect of initial water content on the chemical evolution of residual melt with decreasing temperature. No experimental data is available below 800°C.

Figure 4:

Results of rhyolite-MELTS simulations for dacitic magma. The colors show different initial water content of the magma, from 1 wt.% H_2O (red line) to H_2O saturated (black line). (a) Evolution of the residual melt water content as function of temperature. (b) Relationship between water content of the residual melt and melt fraction. (c) Silica content of the residual melt versus temperature. d) Water content versus silica content of the residual melt.

Figure 5:

Physical parameters of hydrous dacitic magma during melt evolution from rhyolite-MELTS simulations. (a) Temperature decreases with decreasing melt fraction. (b) Evolution of melt viscosity during magma crystallization of H_2O-saturated and undersaturated dacitic magma. (c) The density difference between crystals and the residual melt is large near the liquidus temperature but becomes less pronounced towards lower melt fractions. (d) Relative time magma spends within each fraction interval based on enthalpy budget.

Figure 6:

Hindered settling velocities (Bachmann and Bergantz, 2004) of dacitic magma with different initial water content (H_2O_i). Physical properties are obtained from rhyolite-MELTS simulations. Melt segregation is most effective for hindered settling at its maximum melt fractions of 0.5-0.6. Magmas with $H_2O_i \geq 3$ wt .% segregate at the same rate below a melt fraction of 0.55. Magmas with lower initial water contents have velocities of up to one magnitude lower. All velocities are calculated for a fixed crystal size (i.e. radius) of 3 mm.

Figure 7:

Simulations of residual melt extraction within rheologically locked window for different initial water contents, reservoir volumes (V) and thicknesses (Th). Each line represents one calculation and the cumulative distance travelled by the residual melt for a given reservoir thickness (numbers next to the colored lines).

Figure 8:

a) Regime diagram showing the regions of H_2O_i and thickness of the magma reservoir best suited for the formation of melt caps or lenses. For water content of 1 wt.% there is essentially no significant residual melt segregation before solidification. The dashed lines separate the field where melt caps (below or to the right of the line) and melt lenses (above or to the left of the line) for magmas with different H_2O_i. For higher H_2O_i the potential of forming melt caps increases with increasing reservoir volume. Grey zones indicate regions where melt lenses may form instead of melt caps.

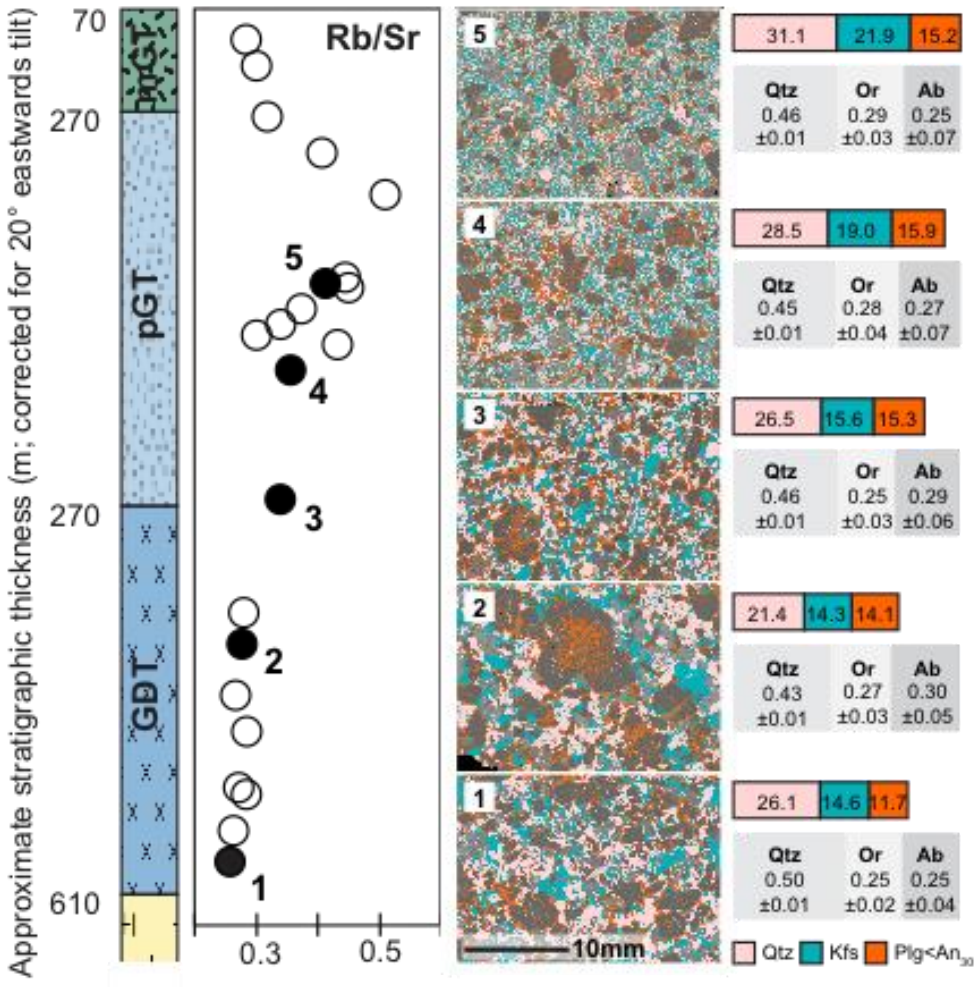
Approximate stratigraphic thickness (m; corrected for 20° eastwards tilt)
70
270
270
610
pGT
GDT
Rb/Sr
0.3
0.5
5
4
3
2
1
10mm
31.1 21.9 15.2
Qtz 0.46 ±0.01
Or 0.29 ±0.03
Ab 0.25 ±0.07
28.5 19.0 15.9
Qtz 0.45 ±0.01
Or 0.28 ±0.04
Ab 0.27 ±0.07
26.5 15.6 15.3
Qtz 0.46 ±0.01
Or 0.25 ±0.03
Ab 0.29 ±0.06
21.4 14.3 14.1
Qtz 0.43 ±0.01
Or 0.27 ±0.03
Ab 0.30 ±0.05
26.1 14.6 11.7
Qtz 0.50 ±0.01
Or 0.25 ±0.02
Ab 0.25 ±0.04
Qtz
Kfs
Plg<An30

535

536

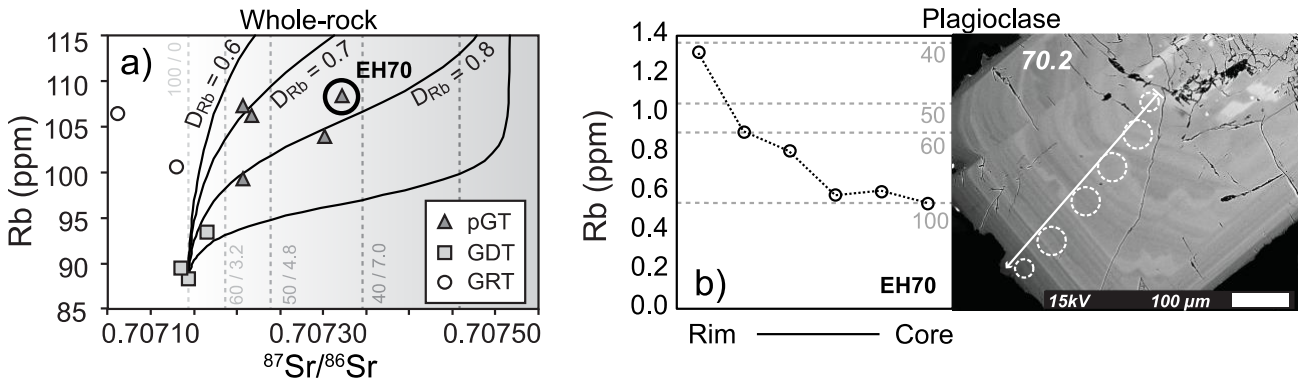
Whole-rock
a)
Rb (ppm)
115
110
105
100
95
90
85
0.70710
0.70730
0.70750
87Sr/86Sr
DRb = 0.6
DRb = 0.7
DRb = 0.8
EH70
100 / 0
60 / 3.2
50 / 4.8
40 / 7.0
pGT
GDT
GRT
Plagioclase
b)
Rb (ppm)
1.4
1.2
1.0
0.8
0.6
0.4
0.2
0.0
40
50
60
100
EH70
Rim
Core
70.2
15kV
100 µm

537

538

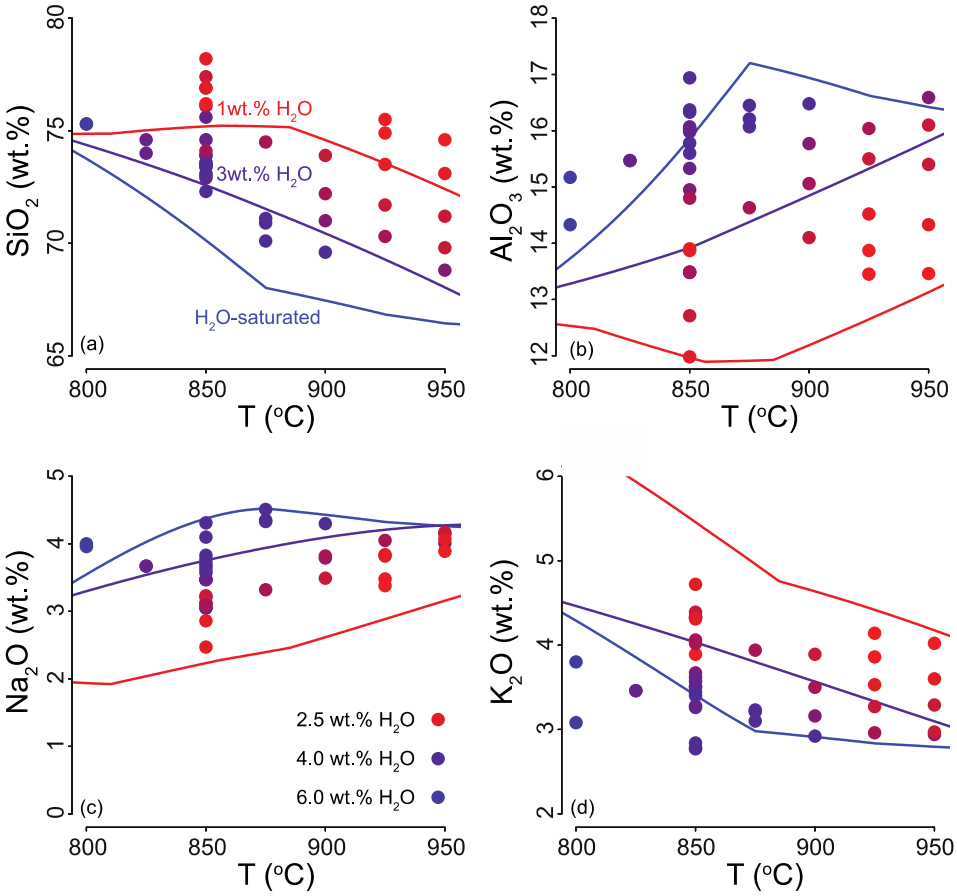
SiO2 (wt.%)
1wt.% H2O
3wt.% H2O
H2O-saturated
(a)
T (°C)
Al2O3 (wt.%)
(b)
Na2O (wt.%)
2.5 wt.% H2O
4.0 wt.% H2O
6.0 wt.% H2O
(c)
K2O (wt.%)
(d)

539

540

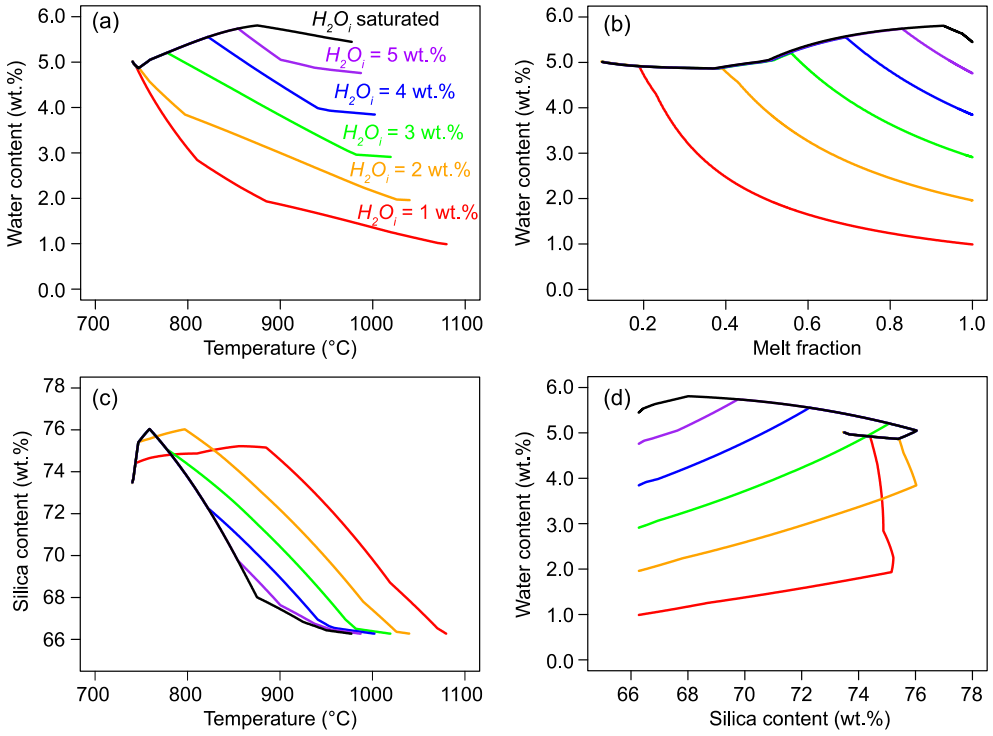
(a)
H_2O_i saturated
H_2O_i = 5 wt.%
H_2O_i = 4 wt.%
H_2O_i = 3 wt.%
H_2O_i = 2 wt.%
H_2O_i = 1 wt.%
Water content (wt.%)
Temperature (°C)
(b)
Water content (wt.%)
Melt fraction
(c)
Silica content (wt.%)
Temperature (°C)
(d)
Water content (wt.%)
Silica content (wt.%)

541

542

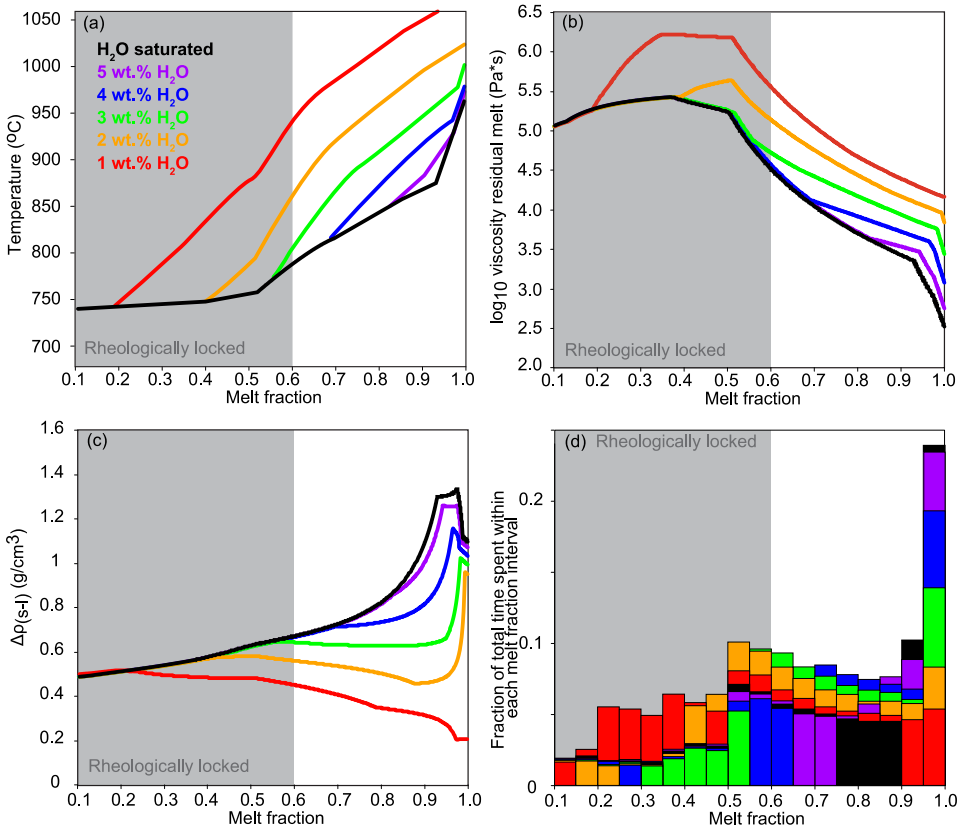
(a)
H2O saturated
5 wt.% H2O
4 wt.% H2O
3 wt.% H2O
2 wt.% H2O
1 wt.% H2O
Temperature (°C)
Rheologically locked
Melt fraction
(b)
log10 viscosity residual melt (Pa*s)
Rheologically locked
Melt fraction
(c)
Δρ(s-l) (g/cm3)
Rheologically locked
Melt fraction
(d) Rheologically locked
Fraction of total time spent within each melt fraction interval
Melt fraction

543

544

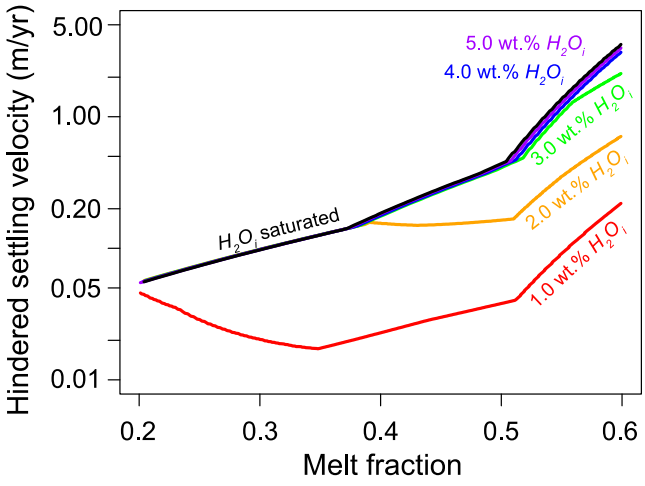
Hindered settling velocity (m/yr)
5.00
1.00
0.20
0.05
0.01
0.2
0.3
0.4
0.5
0.6
Melt fraction
5.0 wt.% H_2O_l
4.0 wt.% H_2O_l
3.0 wt.% H_2O_l
2.0 wt.% H_2O_l
1.0 wt.% H_2O_l
H_2O_l saturated

545

546

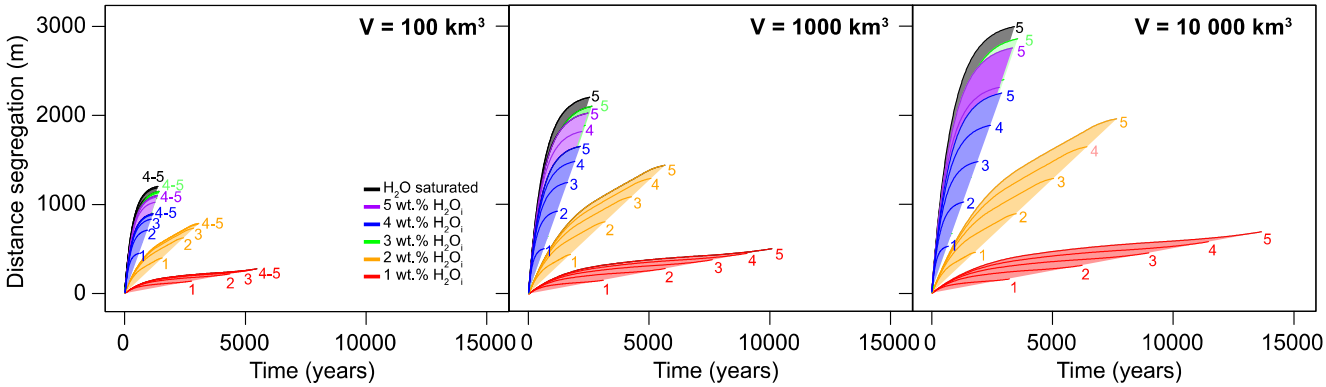
V = 100 km³
V = 1000 km³
V = 10 000 km³
Distance segregation (m)
Time (years)
H2O saturated
5 wt.% H2Oi
4 wt.% H2Oi
3 wt.% H2Oi
2 wt.% H2Oi
1 wt.% H2Oi

547

548

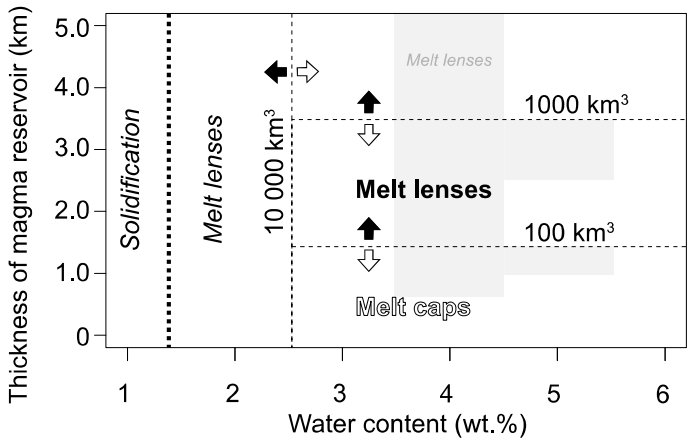
Thickness of magma reservoir (km)
5.0
4.0
3.0
2.0
1.0
0
1
2
3
4
5
6
Water content (wt.%)
Solidification
Melt lenses
10 000 km³
Melt lenses
1000 km³
Melt lenses
100 km³
Melt caps

549